

# Adaptive Reservoir Operation Rules Under Climatic Change

Mohsen Ahmadi · Omid Bozorg Haddad ·  
Hugo A. Loáiciga

Received: 28 February 2014 / Accepted: 30 October 2014 /  
Published online: 9 November 2014  
© Springer Science+Business Media Dordrecht 2014

**Abstract** Increases in greenhouse gases caused by human activities have raised global temperature. Global warming affects water resources systems and the hydrologic cycle and may impact the performance of water resource systems. Water resources managers face challenges balancing conflicting goals in reservoir operation given the uncertainties introduced by climatic change. The HadCM3 climate model is used in this paper to estimate temperature and precipitation for early (2025–2039), middle (2055–2069) and late (2085–2099) periods of the 21st century under the A2 greenhouse gases emission scenario. The estimated temperature and precipitation from the climate model are input to a calibrated hydrologic model (IHACRES) to simulate inflow in a river basin draining to the Karoon-4 reservoir in Iran. A meta-heuristic multi-objective optimization algorithm (NSGA-II) is used in conjunction to predicted hydrologic variables to optimize dynamic operation rules in the Karoon-4 reservoir. The Karoon4 reservoir is operated non-adaptively and adaptively under climatic change. Our results show that adaptive reservoir management increases the reliability and reduces the vulnerability associated with hydropower generation in early, middle, and late simulation periods of the 21st century. These findings establish the importance of factoring in climatic change and considering adaptive strategies in future reservoir operations.

**Keywords** Climatic change · Real-time reservoir operation · Multi-objective optimization · Pareto solutions · Adaptive reservoir operation

---

M. Ahmadi  
Department of Irrigation & Reclamation Engineering, Faculty of Agricultural Engineering & Technology,  
College of Agriculture & Natural Resources, University of Tehran, Karaj, Tehran, Iran  
e-mail: Ahmadi\_M@ut.ac.ir

O. B. Haddad (✉)  
Department of Irrigation & Reclamation Engineering, Faculty of Agricultural Engineering & Technology,  
College of Agriculture & Natural Resources, University of Tehran, Karaj, Tehran, Iran  
e-mail: haddad@iust.ac.ir

H. A. Loáiciga  
Department of Geography, University of California, Santa Barbara, CA 93106, USA  
e-mail: Hugo.Loaiciga@ucsb.edu

## 1 Introduction

The rapid rise in greenhouse gases (GHG) in the atmosphere since the onset of the Industrial Revolution has led to increases in the global average surface temperature of 0.61 °C from the base period 1850–1900 through the comparison period 1986–2005 (Intergovernmental Panel on Climate Change –IPCC, 2014). Rising global temperature affects key hydrologic variables, such as precipitation and evaporation at regional scales (IPCC 2014), which could have a variety of impacts on water resources worldwide. Research findings have revealed that changes in surface temperature and precipitation characteristics (duration, intensity, form, and timing of precipitation) could affect river flows (Loáiciga et al. 1996; Muzik 2001; Boyer 2010), and the management of water resources (Yu 2002; Jiang 2007; Majone 2012; Ashofteh 2013a). Simulated future temperature and precipitation are used in conjunction with suitable hydrologic models and state-of-the-art optimization models to assess the performance of water resources systems under changing climatic conditions. Coupled Atmospheric-Ocean General Circulation Models (AOGCM) are the best tools currently available for predicting future climatic variables (Wilby and Harris 2006).

Reservoir operation depends on lake precipitation, evaporation, and on river inflows (see Loáiciga 2002), which are impacted by changing climate. The impact that climatic change might have on reservoir operation is now well recognized by water resources analysts. This recognition has encouraged the search for new strategies to adapt to and mitigate possible adverse consequence of climatic change.

Numerous optimization techniques have been developed and applied in all areas of water resources systems, and, in particular, in reservoir operation (Bozorg Haddad et al. 2011a; Fallah-Mehdipour et al. 2011a, 2012a, 2013a), hydrology (Orouji et al. 2013), project management (Bozorg Haddad et al. 2010a; Fallah-Mehdipour et al. 2012b), cultivation rules (Bozorg Haddad et al. 2009; Noory et al. 2012; Fallah-Mehdipour et al. 2013b), pumping scheduling (Bozorg Haddad et al. 2011b), hydraulic structures (Bozorg Haddad et al. 2010b), water distribution networks (Bozorg Haddad et al. 2008; Fallah-Mehdipour et al. 2011b; Seifollahi-Aghmiuni et al. 2011, 2013), operation of aquifer systems (Loáiciga 2004; Bozorg Haddad and Mariño 2011), site selection of infrastructures (Karimi-Hosseini et al. 2011), and algorithmic developments (Shokri et al. 2013). Only a handful of these works dealt with the development and application of adaptive reservoir operation rules under climatic change.

Lee et al. (2011) applied a simulation-operation method for finding a tradeoff between flood control and reservoir recharge objectives under a climatic change scenario in the Colombia river watershed. Minville (2009) reported on the adaptive management of Canadian water resources systems under climatic change scenario for hydro-power operation. They investigated the impact of climate change on hydro-power generation, power station performance, weirs and reservoir reliability using a regional climate model (RCM) with the A2 GHG emission scenario.

The operation of multi-objective water resources systems is a complex decision making problem commonly involving many decision variables and multiple objectives. The impact that climatic change might have on reservoir operating variables would further add to the complexity of decision making. Water resources analysts are by now routinely considering climatic change scenarios in planning future multiple reservoir operation strategies (Lee et al. 2011).

Eum and Simonovic (2010) proposed a new strategy for adapting multi-objective reservoirs to climatic change using optimized operation rule curves using the Differential Evolution Optimization (DEO) algorithm. They weighted water supply, flood

control, and hydropower generation objectives to calculate reservoir operation rule curves under climatic change. Zhou and Guo (2013) proposed an integrated optimization model to develop operation rule curves for the Danjiangkou reservoir in China in a base period and three future periods.

It is now recognized by many professionals in the water resources community that reservoir operation rules must take into account climatic change. This work presents an adaptive method to revise reservoir operation rules as an adaptation strategy to climatic change. The method is illustrated with an application to the Karoon-4 reservoir in Iran.

## 2 Methodology

### 2.1 Climate Scenarios

The preferred tool to generate future climate scenarios is the coupled Atmospheric-Ocean General Circulation Model (AOGCM) (Mithcell 2003; and Wilby and Harris 2006). The path of future GHG emissions is an input to AOGCMs. A set of emission scenarios titled Special Report on Emission Scenarios (SRES) was released by the IPCC in 1996 and updated in 2000 (IPCC 2000). Scenarios are allocated to four main groups: A1, A2, B1 and B2. The A2 scenario of GHG emissions, which is adopted in this work, envisions a heterogeneous world, continuously increasing global population, economic development is primarily regionally oriented, with slow per capita economic growth and technologic change. There are different techniques to generate regional climate scenarios from AOGCM climatic output computed at larger spatial resolution. These methods are known as downscaling techniques (Wilby and Harris 2006). The proportional approach is adopted in this work for spatial downscaling of AOGCM output. This approach downscales climate change scenarios to the basin using the information of the AOGCM's grid box or boxes that contain the basin under study.

The 'change fields' temporal downscaling approach is used in this work to generate monthly climatic scenarios. In this approach, monthly differences (or ratios) are formed between the averages of the AOGCMs outputs dataset for the future and the corresponding averages of the models simulated for a base period. The differences [Eq. (1)] are used for temperature changes and ratios (Eq. 2) are commonly applied to rainfall change (Loáiciga et al. 2000; Hay 2000; Diaz-Nieto and Wilby 2005; Minvill 2008 and Ashofteh 2013b). The differences and ratio approaches are as follows:

$$\Delta T_t = \left( \bar{T}_{AOGCM, fut, t} - \bar{T}_{AOGCM, base, t} \right) \quad (1)$$

$$\Delta P_t = \left( \frac{\bar{P}_{AOGCM, fut, t}}{\bar{P}_{AOGCM, base, t}} \right) \quad (2)$$

in which  $\Delta T_t$  and  $\Delta P_t$  = long-term monthly average temperature and precipitation changes for month  $t$ , respectively;  $\bar{T}_{AOGCM, fut, t}$  and  $\bar{P}_{AOGCM, fut, t}$  = the simulated long-term average temperature and precipitation with an AOGCM in future periods for month  $t$ , respectively;  $\bar{T}_{AOGCM, base, t}$  and  $\bar{P}_{AOGCM, base, t}$  = the simulated long-term average temperature and precipitation by AOGCM in the base period for the month  $t$ , respectively.

The future (monthly) temperature time series ( $T_t$ ) is calculated by adding the change in temperature obtained with Eq. (1) to the temperature observed during a baseline period ( $T_{obs,t}$ ):

$$T_t = T_{obs,t} + \Delta T_t \tag{3}$$

The future (monthly) time series of precipitation ( $P_t$ ) is calculated by multiplying the change of precipitation obtained with Eq. (2) by the precipitation observed during a baseline period ( $P_{obs,t}$ ):

$$P_t = P_{obs,t} \times \Delta P_t \tag{4}$$

### 2.2 Future Runoff Under Climate Change

Basin runoff must be predicted to evaluate the future impacts of climate change on water resources. This is accomplished in this work by means of the rainfall-runoff model IHACRES, which is versatile, computationally efficient, and can be interfaced with climate-change input data.

### 2.3 The IHACRES Model

The IHACRES model was introduced by Jakeman and Hornberger (1993). This model is based on a non-linear loss module and a linear unit hydrograph module. Precipitation  $P_t$  and temperature  $T_t$  are converted to effective precipitation  $u_t$  using the non-linear loss module in every time step  $t$ . The linear module unit hydrograph then converts effective precipitation to runoff in every time step. The catchment wetness index  $s_t$  ( $0 < s_t < 1$ ) is used to convert precipitation to effective rainfall in a catchment. The catchment wetness index is a function of evaporation and is shown as follows:

$$s_t = C \times r_t + \left(1 - \frac{1}{\tau_w(T_t)}\right) s_{t-1} \tag{5}$$

in which  $P_t$ =the catchment precipitation in period  $t$ ,  $u_t$ =the effective rainfall in period  $t$ . If the soil in the catchment is completely saturated ( $s_t=1$ ) all precipitation is converted to effective rainfall.  $\tau_w(T_t)$  is a parameter that controls the value of the  $s_t$  index when no precipitation occurs. It is calculated as follows:

$$\tau_w(T_t) = \tau_w e^{0.062f(R-T_t)} \tag{6}$$

in which  $R$ =reference temperature,  $\tau_w$  = catchment drying time constant,  $f$ =the temperature modulation factor. The effective rainfall  $u_t$  is the product of  $P_t$  and  $s_t$ :

$$u_t = s_t \times P_t \tag{7}$$

The linear module allows any configuration of linear storages acting in parallel or in series. In a two-storage configuration the unit hydrograph is divided into quick (q) and slow (s) components. The value of runoff in the time step  $t$  ( $q_t$ ) is estimated using the following equation (Jakeman and Hornberger 1993)

$$q_t = \left(\alpha^{(q)} x_{t-1}^{(q)} + \beta^{(q)} u_t^{(q)}\right) + \left(\alpha^{(s)} x_{t-1}^{(s)} + \beta^{(s)} u_t^{(s)}\right) \tag{8}$$

The three parameters  $C$  [Eq. (5)],  $\tau_w$ , and  $f$  [Eq. (6)] and the four parameters  $\alpha^{(q)}$   $\alpha^{(s)}$   $\beta^{(s)}$  or  $\beta^{(q)}$  (Eq. 8) must be calibrated using observed data for the study basin.

### 3 Reservoir Operation Model

#### 3.1 Multi-objective Optimization Model

Multiobjective optimization seeks to achieve the best possible fulfillment of all the objectives of reservoir operation simultaneously. The objective functions used in this study are the temporal reliability and vulnerability of hydropower generation, following earlier work by Ahmadi (2014).

The reliability of hydropower generation is defined as follows:

$$RT = \frac{\sum_{t=1}^T (P_t \geq \alpha \cdot PPC)}{T} \tag{9}$$

The vulnerability of hydropower generation is defined as follows:

$$V = \frac{\sum_{t=1}^T (\alpha \cdot PPC - P_t | P_t < \alpha \cdot PPC, 0 | P_t \geq \alpha \cdot PPC)}{T \cdot \alpha \cdot PPC} \tag{10}$$

in which  $RT$  = temporal reliability of reservoir;  $\alpha$  = efficiency threshold of hydropower generation;  $P_t$ =hydropower generation at period  $t$ ;  $PPC$ =existing power plant capacity;  $V$ =vulnerability of the reservoir; and  $T$ =total number of operational periods.

Other equations and additional relevant constraints for single reservoir optimization models are as follows:

Water balance equation in the reservoir:

$$S_{t+1} = S_t + Q_t - R_t - Sp_t - Loss_t (\forall t = 1, \dots, T) \tag{11}$$

in which  $S_t$  and  $S_{t+1}$ =reservoir storage volume at the beginning of the  $t^{th}$  and  $t+1$ st periods, respectively;  $Q_t$ =river inflow volume to reservoir during period  $t$ ;  $R_t$ =volume of water released from the reservoir during period  $t$ ;  $Sp_t$ =volume of spilled water from the reservoir during period  $t$ ;  $Loss_t$ =volume of evaporation losses from the reservoir during period  $t$ .

Loss equation:

$$Loss_t = Ev_t \times \left( \frac{A_t + A_{t+1}}{2} \right) (\forall t = 1, \dots, T) \tag{12}$$

in which  $Ev_t$ =evaporation depth at period  $t$ ;  $A_t$  and  $A_{t+1}$ =water surface at the beginning of  $t^{th}$  and  $t+1$ st periods, respectively.

Area-storage function:

$$A_t = f(S_t) (\forall t = 1, \dots, T) \tag{13}$$

in which  $f(\dots)$  = area-storage function.

Spill function:

$$Sp_t = \begin{cases} S_t + Q_t - R_t - S_{max} & \text{if } S_t + Q_t - R_t > S_{max} \\ 0 & \text{if } S_t + Q_t - R_t \leq S_{max} \end{cases} (\forall t = 1, \dots, T) \tag{14}$$

in which  $S_{min}$  and  $S_{max}$ =minimum and maximum storage of the reservoir, respectively.

Constraint on storage:

$$S_{\min} \leq S_t \leq S_{\max} (\forall t = 1, \dots, T) \tag{15}$$

Constraint on releases:

$$R_{\min} \leq R_t \leq R_{\max} (\forall t = 1, \dots, T) \tag{16}$$

in which  $R_{\min}$  and  $R_{\max}$ =minimum and maximum allowable reservoir releases, respectively.

Power formula:

$$P_t = g \times E \times \frac{Rp_t}{PF_t \times Mul_t} \times \frac{(\bar{H}_t - Tw_t)}{1000} (\forall t = 1, \dots, T) \tag{17}$$

in which  $g$ =gravitational acceleration;  $E$ =power plant efficiency;  $Rp_t$ =output water from power plant in period  $t$ ;  $PF_t$ =plant functional coefficient during period  $t$ ;  $\bar{H}_t$  = average head during period  $t$ ;  $Tw_t$ =reservoir tailwater level during period  $t$  that depends on output water from the power plant.

Average head formula:

$$\bar{H}_t = (H_t + H_{t+1})/2 (\forall t = 1, \dots, T) \tag{18}$$

in which  $H_t$  and  $H_{t+1}$ =head at the beginning of  $t^{th}$  and  $t+1$ th periods, respectively.

Head vs. storage function:

$$H_t = g(S_t) (\forall t = 1, \dots, T) \tag{19}$$

in which  $f(\dots)$  = head-storage function.

Definition of spill from the power plant:

$$Rps_t = R_t - Rp_t (\forall t = 1, \dots, T) \tag{20}$$

in which  $Rps_t$ =additional water spilled from the power plant after hydropower generated in period  $t$ .

Power plant capacity constraint:

$$P_{\min} \leq P_t \leq PPC (\forall t = 1, \dots, T) \tag{21}$$

In which  $P_{\min}$ =minimum hydropower generation of plant.

### 3.2 Dynamic Real-Time Reservoir Operation Rules

Reservoir operation rules can be either long term or real time. In long-term operation, a reservoir is operated with a historical long-term series of inflow. In real-time operation the released water from a reservoir in each period is a function of variables such as reservoir storage volume at the beginning of the current period or the end of previous period, the reservoir inflow during the current period, and downstream requirements during the current period. In fact, in real-time operation the operator consider combinations of inflow volume, reservoir volume, and released water volume to make the final operational decision for the current period. The volume of released water can be a linear or non linear function of storage volume, inflow volume, or both of these variables.

The volumes of river inflows over different time periods are unknown in real-time operation: their volumes are estimated using inflow forecasting models. The application of

inflow forecasting models may be beset by large errors. As an alternative, real-time operation rules may be such that the volume of released water in each period is a function of the volume of reservoir storage at the beginning of the current period and on the volume of inflow of the previous period, which are known values (Ahmadi 2014). Inflow forecasting model is not needed for the real-time operation rules in this instance. Using this method, real-time operation rules are expressed by Eq. (22). In this case, a separate inflow forecasting model is not needed for the real-time operation rules.

$$R_t = j(S_t, Q_{t-1}) (\forall t = 1, \dots, T) \quad (22)$$

in which  $j(\dots)$  denotes the function relating the water release in period  $t$  to storage in period  $t$  and inflow in period  $t-1$ .

The amount of water released in period  $t$  is expressed by Eq. (23) (see Ahmadi 2014):  $x_1$ ,  $x_2$  and  $x_3$ , for each month and a total of 36 variables during operation.

$$R_t = x_1 \cdot S_t + x_2 Q_{t-1} + x_3 (\forall t = 1, \dots, T) \quad (23)$$

in which  $x_{1t}$ ,  $x_{2t}$  and  $x_{3t}$  are storage, river inflow, and free coefficients, respectively, in the operation rule (23). These coefficients differ from month to month but are fixed for each given month of the year, so that their total number equals 36 ( $3 \times 12$ ). The coefficients  $x_1$ ,  $x_2$  and  $x_3$  are treated as decision variables in reservoir optimization in this work. These coefficients introduce flexibility in setting up operation rules leading to improved real-time dynamic operation rules.

### 3.3 Multi-objective Optimization Algorithm

Multiobjective reservoir operation rules can be optimized using meta-heuristic algorithms (Zhou and Guo 2013). The non-dominated sorting genetic algorithm II (NSGA-II) (Deb 2002) was chosen as the multi-objective optimization problem solver in this work. In the NSGA-II algorithm each population consists of genes that are the decision variables of the optimization model. The choice of a new population in each phase of this algorithm is based on the concepts of dominance, elitism, and population ranking. The algorithm chooses non dominant solutions in each phase and moves to the next phase. The algorithm assures an appropriate distribution of solutions using the concept of Crowding Distance (Deb 2002).

Output of all multi-objective optimization methods is a set of optimal solutions that are called Pareto optimal solutions (Pareto frontier). The Pareto frontier consist a set of non-dominated solutions which are near the optimal solutions for any combination of objectives with an appropriate diversity. All of these optimal solutions are potentially the final choice and the decision maker should choose one of them as a final solution. There are several methods that can be employed to select a final solution among the Pareto set. Young's (1993) theory can be used to resolve conflicts among objectives in optimal reservoir operation (Shokri et al. 2014).

### 3.4 Approach to Reservoir Operation

This paper investigates the impact of climate change on real time, multiobjective, reservoir operation. Temperature and precipitation data were extracted from the HadCM3 climate model (Pope et al. 2000) predicted under the A2 emission scenario for the base period (1986–2000) and for the early (2025–2039), middle (2055–2069), and late (2085–2099) periods. The climate model's predictions were used to generate river inflows to the Karoon-4 reservoir with the IHACRES rainfall simulation model.

Dynamic multi-objective real-time operation rules are herein described by Eq. (23). The temporal reliability [Eq. (1)] and the vulnerability [Eq. (2)] of hydropower generation are the two objective functions of this study. The multi-objective optimization of real-time operation is performed using the NSGA-II. Due to the random nature of the solutions obtained with the NSGA-II the optimization model was run six times, and final Pareto solutions were chosen from the non-dominated solutions of all the runs. The NSGA-II parameters include crossover rate, mutation rate, population size, and number of generations. These parameters are chosen using sensitivity analysis. The optimum value of each parameter is determined by changing one parameter within its allowable range while the other parameters are kept constant. The crossover rate, mutation rate, population size, and number of generations were estimated to be equal to 0.1, 8, 100, and 30000, respectively. Maximum reliability and minimum vulnerability were also obtained with the software LINGO by performing single-objective optimization of each objective function and compared with the multiobjective Pareto solutions. Figure 1 shows a flowchart of the solution methodology employed in this work.

### 3.5 Case Study

The Karoon-bala basin, Iran, has an area of about 14,550 km<sup>2</sup> and mean elevation of 2,300 m. It is located in southwestern Iran (see Fig. 2). The 240 km-long Karoon

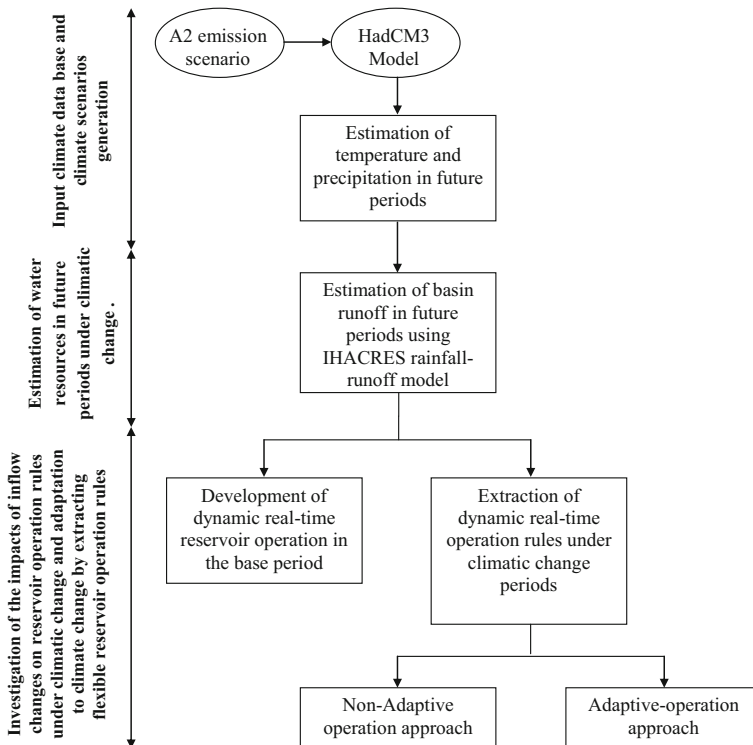


**Fig. 1** Flowchart of the reservoir operation methodology



river lies in this basin. The Karoon river has the largest discharge among all rivers in Iran. The concrete, double curvature, arch-type Karoon-4 dam has a height of 230 m. It is the tallest dam in Iran, and is located at the outlet of the Karoon basin. The objectives of the Karoon-4 dam and hydroelectric power plant are water supply ( $7.3 \times 10^9 \text{ m}^3$  per year), flood control, and annual hydropower production (2,107 GWhr per year). The mean annual river discharge and rainfall at the Karoon-4 reservoir are  $540 \times 10^6 \text{ m}^3$  and 620 mm, respectively. The years 1986–2000 were selected as the base period in this study. Monthly rainfall (from 13 stations), temperature (from 2 stations), and monthly river discharge (from hydrometer gauging station at Karoon-4 reservoir) are available for the base period.

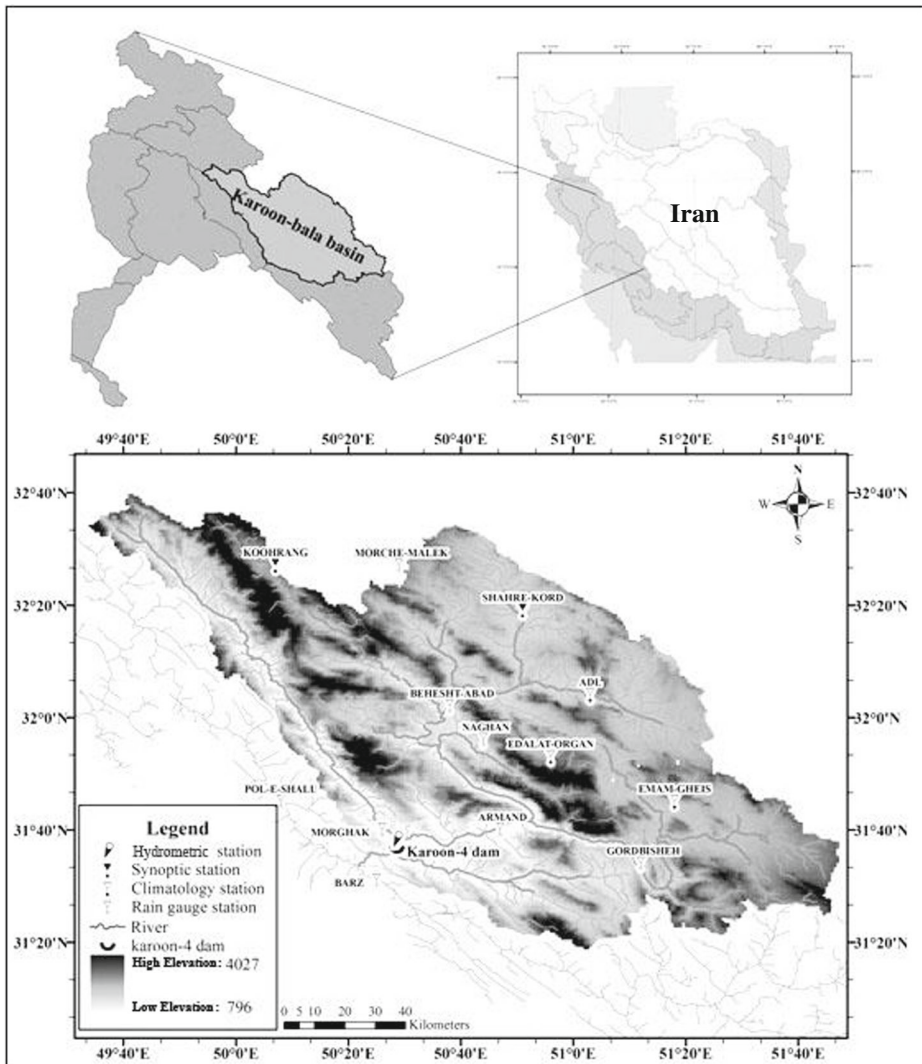


**Fig. 2** Location of the study basin and stations

### 4 Results and Discussion

#### 4.1 Investigation of Climate Model Performance in the Base Period (1986–2000)

15-year average monthly precipitation and temperature downscaled from HadCM3 model predictions are compared to the 15-year average monthly observed precipitation and temperature in Fig. 3 for the base period at the Karoon-4 reservoir. Climate predictions for temperature and precipitations at the Karoon-4 reservoir were calculated with Eqs. (3) and (4), respectively. As shown in the Fig. 3, the HadCM3 model predicted average temperature that are lower than observed temperature in most months, while it yielded an estimated average precipitation greater than observed precipitation in several months. The correlation coefficient ( $r$ ), root mean square error (RMSE), and mean absolute error (MAE)) of precipitation and temperature predictions are listed in Table 1. The results show that the HadCM3 model produced acceptable climate predictions for the purpose of this study.

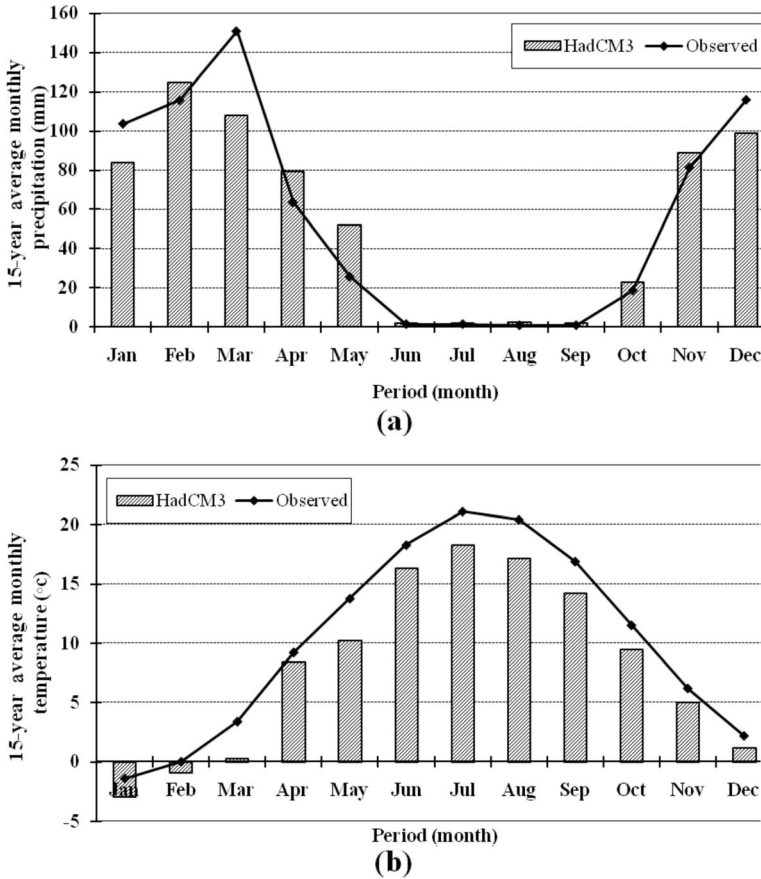


**Fig. 3** 15-year average monthly **a** temperature, **b** precipitation of observed data and HadCM3 predictions for the base period (1986–2000)

**Table 1** Performance criteria of the HadCM3 model for temperature and rainfall observed data

Performance criteria	Precipitation			Temperature		
	<i>r</i> (%)	<i>RMSE</i> (mm)	<i>MAE</i> (mm)	<i>r</i> (%)	<i>RMSE</i> (°c)	<i>MAE</i> (°c)
HadCM3	89	4.69	-2.29	99	1.14	1.92

4.2 Prediction of Climate Variables in Future Periods

Figure 4 shows the long-term average monthly temperature and precipitation predictions for the early (2025–2030), middle (2055–2069), and late (2085–2099) periods. The base period predictions are displayed for comparison purposes in Fig. 4, also.

Figure 4a shows that future periods exhibit higher temperature than the base period. The early, middle and late periods exhibit basin temperatures that are 1.35, 1.45, and 2.20 °C higher than the base period temperature, respectively. Figure 4b shows that the amount of

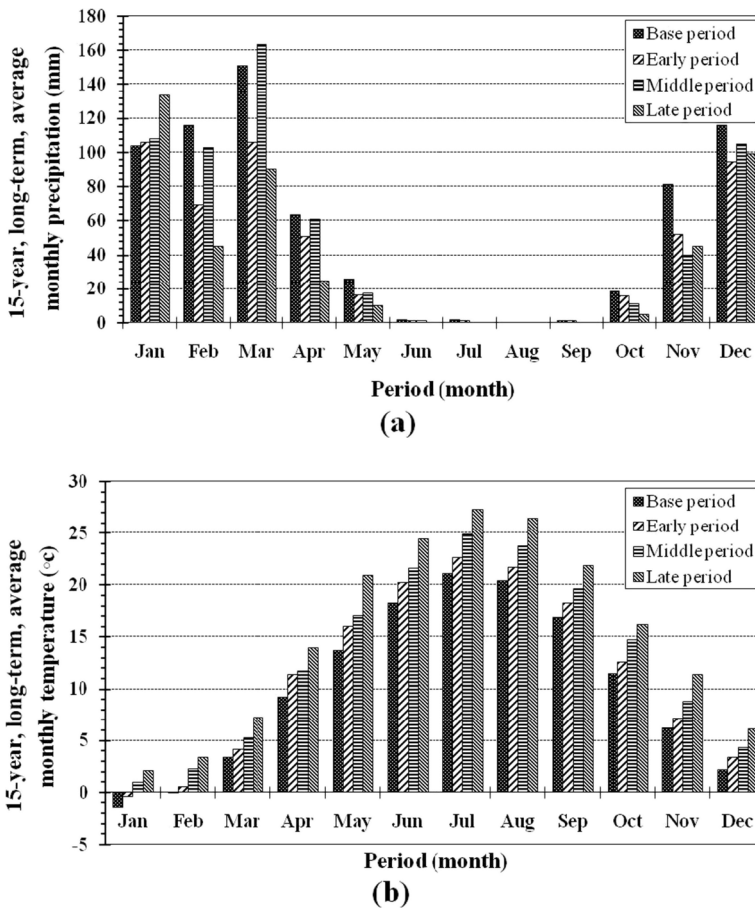


**Fig. 4** 15-year, long-term, average monthly temperature **a** and precipitation **b** in the Karoon basin for the base period and future periods

precipitation decreases by 18 % in the early period, 0.4 % in the middle period, and 30 % in the late period relative to the base period. An increase in precipitation is observed only in the Winter and Spring seasons of the middle period. The precipitation decreases relative to the base period in the other periods.

#### 4.3 Prediction of Basin Runoff in Future Periods

The IHACRES hydrologic model was calibrated using observed monthly average temperature and precipitation data for the basin, and Karoon-4 monthly runoff data during 1986–2000. Figure 5 shows partial calibration and verification results. The calibrated IHACRES model was simulated with inputs of predicted monthly precipitation and runoff to simulate predicted runoff at the Karoon-4 reservoir. Results are shown in Fig. 6.

Figure 6 indicates a decrease in river inflow to the Karoon4 reservoir in the future periods relative to the base period. The middle period has smaller decrease than the early period, and the late period has the largest decrease in inflow relative to the base period. The middle period exhibits decreases in river inflow that are smaller than those in the early period.

#### 4.4 Real-Time Reservoir Operation in the Base Period

The Karoon-4 reservoir was operated by extracting dynamic real-time operation rules for the base period. These rules were optimized using a two-objective problem that maximizes reliability and minimizes vulnerability of hydroelectric power generation. Results of the two-objective optimization algorithm are shown in the form of Pareto solutions in Fig. 7. The single-objective optimal values of each objective function were calculated using the LINGO software, and are shown in Fig. 7, also.  $S_I^{base}$  and  $S_{III}^{base}$  in Fig. 7 denote the maximum reliability and minimum vulnerability obtained with LINGO from single-objective optimization of each objective function.

It is seen in Fig. 7 that the Pareto solutions exhibit a good spread in the solutions set, and are near single-objective solutions (absolute optimal solution of each objective function). This indicates appropriate performance of the multi-objective optimization algorithm.

Each of the solutions on the Pareto curve or frontier represents an optimal operation rule which include reservoir release volume, reservoir storage volume, generated hydropower, and volume of spilled water from the reservoir. These variables make up an optimized operation policy. All Pareto optimal solutions are considered equally good. Each of the Pareto solutions

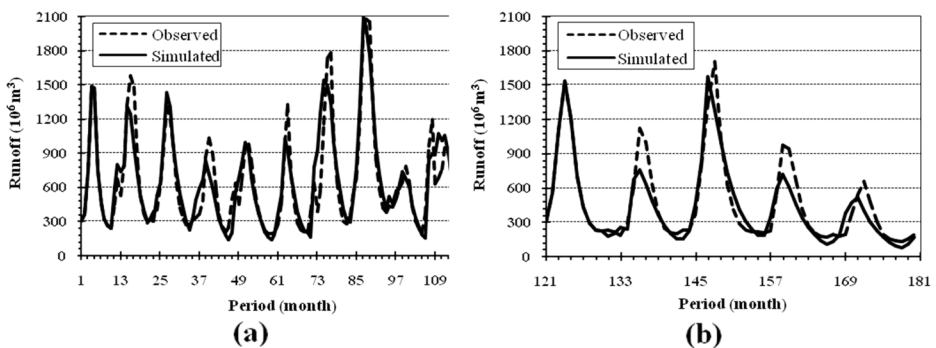


**Fig. 5** Observed and simulated runoff for **a** calibration period ( $r=84\%$ ,  $RMSE=2.01 \times 10^6 \text{ m}^3$  and  $MAE=1.92 \times 10^6 \text{ m}^3$ ), and **b** verification ( $r=73\%$ ,  $RMSE=5.32 \times 10^6 \text{ m}^3$  and  $MAE=2.16 \times 10^6 \text{ m}^3$ ) period

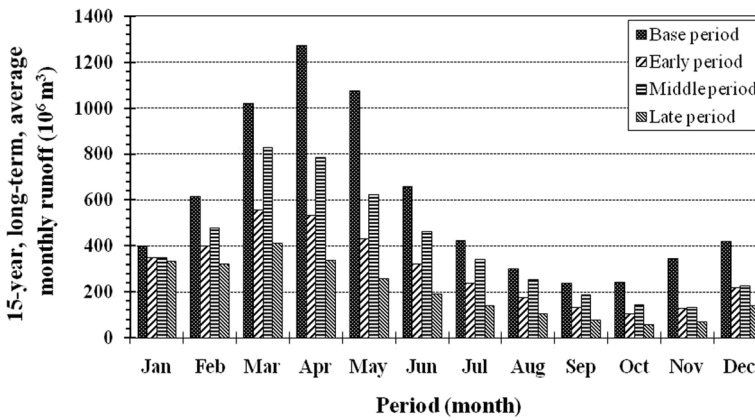


Fig. 6 Average Long-term average monthly runoff observed in the base period and modeled in future periods

can be regarded as an optimal solution and the final choice could be made by the reservoir operator. In this paper, the final optimal decision variables are chosen using Young’s conflict resolution method (Young 1993).  $S_{II}^{base}$  in Fig. 7 denotes the final choice of Pareto solutions, which are selected using Young theory.

Table 2 shows the values of the objective functions and optimized coefficients of storage volume ( $x_1$ ), inflow volume ( $x_2$ ) and constant values ( $x_3$ ) in Eq. (23).

#### 4.5 Real-Time Operation Under Climatic Change Condition in Future Periods

The Karoon4 reservoir can be operated according to two approaches under climate change: (1) non-adaptive operation, and (2) adaptive operation. In the non-adaptive operation approach the developed operational rules in the base period are used for operating the reservoir in future periods, and climate change impacts on reservoir operation are investigated. In the adaptive

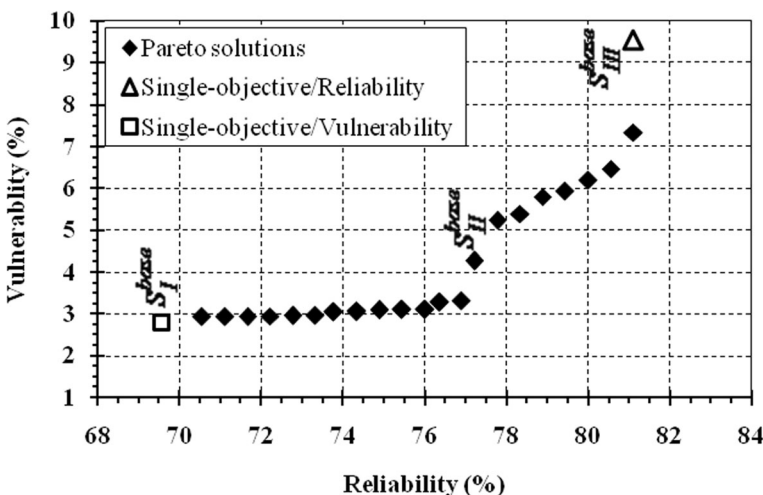


Fig. 7 Pareto optimal solutions of real-time operation in the base period (1986–2000)

**Table 2** Optimal solutions for real-time dynamic operation rules in the base period (1986–2000)

	$S_I^{base}$			$S_{II}^{base}$			$S_{III}^{base}$		
	$x_1$	$x_2$	$x_3$	$x_1$	$x_2$	$x_3$	$x_1$	$x_2$	$x_3$
Reliability (%)	81.11			77.22			2.80		
Vulnerability (%)	9.54			4.27			2.80		
Jan	0.1989	0.2008	61.7720	0.2198	0.0029	281.8914	0.2127	0.0016	288.7750
Feb	0.1443	0.0061	325.4311	0.1210	0.0350	335.9921	0.0467	0.1390	319.9667
Mar	0.0699	0.0360	328.3409	0.0944	0.0699	295.4731	0.0893	0.0052	376.7884
Apr	0.2201	0.0373	206.4848	0.0308	0.0349	314.7803	0.0271	0.0002	328.8053
May	0.3223	0.0464	56.2425	0.1425	0.0656	205.9424	0.3621	0.0194	50.2153
Jun	0.0120	0.0000	306.0391	0.2938	0.0410	85.5548	0.0953	0.0480	224.3974
Jul	0.0463	0.0795	274.8175	0.2165	0.1376	107.7698	0.2556	0.1407	55.1750
Aug	0.1373	0.1739	198.5104	0.2368	0.1177	107.6385	0.0448	0.2943	167.8485
Sep	0.4560	0.0085	96.0059	0.3647	0.0497	72.9243	0.2012	0.0784	154.9512
Oct	0.0142	0.0971	370.1594	0.0038	0.4283	127.6349	0.0747	0.2941	229.6880
Nov	0.0825	0.0534	78.7758	0.0933	0.3727	216.8537	0.3637	0.2470	96.4769
Dec	0.4740	0.0155	59.6035	0.0941	0.1142	260.8091	0.0450	0.1046	308.1980

operation approach dynamic real-time operation rules are modified in future periods for adapting to climate change.

#### 4.6 Non-adaptive Operation Approach

Using the predicted inflow for future periods to the reservoir and the operational rules calculated for the base period, real-time operation in the early (2025–2030), middle (2055–2069), and late (2085–2099) periods was simulated for the optimal solutions  $S_I^{base}$ ,  $S_{II}^{base}$  and  $S_{III}^{base}$  shown in Table 2. Table 3 displays the reliability and vulnerability of hydroelectric power generation obtained from reservoir simulation in the future periods using non-adaptive operation.

It is seen in Table 3 that using operational rules developed in the base period in future periods leads to a decrease in reliability and an increase in vulnerability of hydroelectric power generation. The reliability decreases between 45 and 55 % and the vulnerability increases between 22 and 31 % in the early period, the reliability decreases between 27 and 33 % and the vulnerability increases between 16 and 20 % in the middle period, and the reliability decreases between 59 and 64 %, and the vulnerability increases between 45 and 51 % in the late period.

**Table 3** Non-adaptive real-time operation in the future periods

	$S_I^{early}$	$S_{II}^{early}$	$S_{III}^{early}$	$S_I^{middle}$	$S_{II}^{middle}$	$S_{III}^{middle}$	$S_I^{late}$	$S_{II}^{late}$	$S_{III}^{late}$
Reliability (%)	34.44	18.89	22.22	47.78	40.56	44.44	15.56	6.00	7.78
Vulnerability (%)	40.81	20.87	34.86	28.67	18.16	21.30	58.79	48.11	50.11

#### 4.7 Adaptive-Operation Approach

Operating rules must be modified in the future for best adaptation to climatic change. Simulated volumes of inflow in future periods were input to the optimization model and dynamic optimal rules of reservoir operation were calculated as multi-objective and single-objective for the early, middle and late periods.

Figure 8 shows the Pareto solutions resulting from multi-objective, adaptive, optimization of reservoir operation in the future periods.

The values of the objective functions and decision variables calculated with the optimization model are presented for the early period ( $S_I^{i,early}$ ,  $S_{II}^{i,early}$  and  $S_{III}^{i,early}$ ), middle period ( $S_I^{i,middle}$ ,  $S_{II}^{i,middle}$  and  $S_{III}^{i,middle}$ ) and late period ( $S_I^{i,late}$ ,  $S_{II}^{i,late}$  and  $S_{III}^{i,late}$ ) in Tables 4 to 6, respectively.

A comparison of the adaptive operational results for the future periods shown in Tables 4, 5 and 6 with those presented in Table 2 for the base period establishes that the reliability decreases approximately between 38 and 49 % and the vulnerability increases approximately between 21 and 25 %, in the early period relative to those of the base period. Due to the trend of inflow changes in future periods stated earlier in this paper, the reliability and vulnerability in the middle period exhibit smaller changes than in other future periods relative to those of the base period. Specifically, in the middle period the reliability decreases approximately between 31 and 40 % and the vulnerability increases approximately between 9 and 13 % relative to those of the base period. Results for the late period show a decrease between 52 and 62 % for the reliability and an increase between 42 and 45 % for the vulnerability relative to those of the base period.

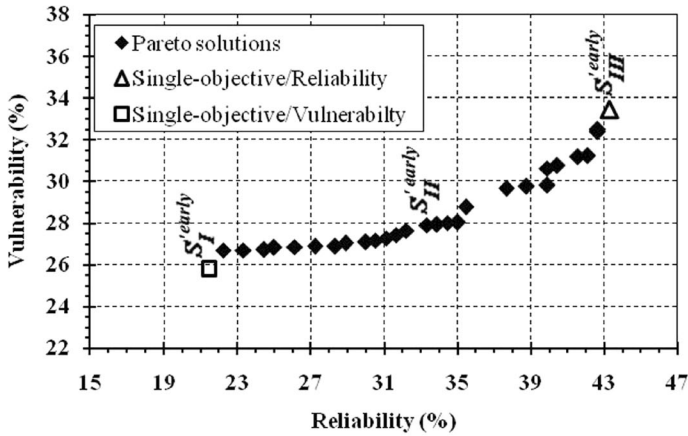
Adaptive operation results can be compared to those calculated with non-adaptive operation. The non-adaptive operating results (Table 3) and the adaptive results for the future periods (Tables 4, 5 and 6) establish that applying the adaptive operational rules in future periods improves the reliability and vulnerability of hydroelectric power generation, so that the adaptive reliabilities  $S_{II}^{i,early}$  and  $S_{II}^{i,middle}$  improve 11 and 4 %, respectively, and their vulnerability improves 7 and 5 %, respectively, relative to non-adaptive  $S_{II}^{early}$  and  $S_{II}^{middle}$ . Hence, changing the reservoir operation rules under climate change in future periods means improved operation, making modification of these rules by applying multi-objective optimization an effective strategy for climatic-change adaptation.

Figure 9 displays the 15-year average monthly values of reservoir release volume, reservoir storage volume, generated hydropower, and the volume of spilled water from the reservoir obtained from the Pareto solutions for the base, early, middle and late periods.

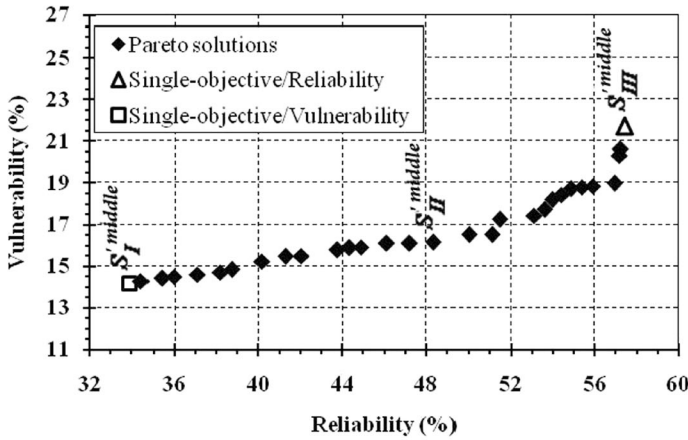
#### 4.8 Concluding Remarks

The HadCM3 model under the A2 scenario was used to predict temperature and precipitation in the Karoon river basin of Iran. The temperature and precipitation predictions were downscaled by the proportional method. Predicted average temperature and precipitation in three future periods -early (2025–2039), middle (2055–2069), and late (2085–2099) were input to the hydrologic model IHACRES to simulate river inflow to the Karoon-4 reservoir. Dynamic real-time operation rules were calculated with the NSGA-II. Lastly, the reservoir was operated under climate change in using non-adaptive and adaptive operations.

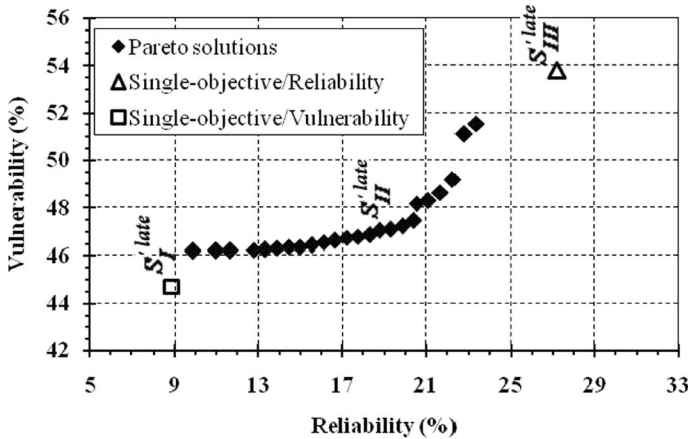
The climatic predictions for the future periods indicate that the basin temperature in the early, middle, and late periods decreases about 1.35, 1.45 and 2.20°C relative to the base period, respectively. Precipitation predictions indicate that it would decrease about 18, 0.4 and 30 % in the early, middle, and late periods, respectively, relative to the base period. Runoff



(a)



(b)



(c)

**Fig. 8** Pareto optimal solutions of real-time operation in **a** early (2025–2030), **b** middle (2055–2060), and **c** late (2085–2099) periods



**Table 4** Optimal adaptive solutions for real-time dynamic operation rules in the early period (2025–2039)

	$S_I^{early}$			$S_{II}^{early}$			$S_{III}^{early}$		
	$x_1$	$x_2$	$x_3$	$x_1$	$x_2$	$x_3$	$x_1$	$x_2$	$x_3$
Reliability (%)	43.30			33.33			21.44		
Vulnerability (%)	33.44			27.92			25.78		
Jan	0.2321	-0.0403	169.4214	0.3086	0.0562	167.7198	0.9409	0.0712	50.5869
Feb	0.0926	-0.0396	305.0996	0.1250	-0.0463	303.3760	0.3955	0.0153	210.4714
Mar	0.4809	-0.1306	59.0741	0.5640	-0.1048	59.5572	-0.1314	0.6107	106.7474
Apr	0.1319	0.2413	86.4134	0.1356	0.2447	86.5448	0.3499	-0.1029	210.8435
May	0.1729	0.0404	182.4676	0.1818	0.0417	182.3326	0.2348	-0.0247	174.9682
Jun	0.1065	0.1183	222.2596	0.0745	0.1180	218.4090	0.1200	-0.0139	236.8797
Jul	0.2550	0.0559	182.0610	0.2388	-0.0412	178.5641	0.5695	-0.8216	184.7130
Aug	0.0305	-0.1527	67.8333	0.2557	-0.0664	68.5082	0.5252	-0.7109	151.2719
Sep	0.3552	-0.9881	96.7164	0.6506	-0.8469	95.9358	0.3775	-0.0480	50.0000
Oct	0.1093	-0.5022	53.0703	0.2559	-0.4874	52.6138	0.5122	-0.1983	50.0001
Nov	0.2134	0.9036	55.8794	0.2212	0.3075	54.1997	0.6859	-0.1466	50.0217
Dec	-0.0842	-0.0101	50.6954	0.0500	0.4753	53.6205	0.4318	0.4476	98.1140

simulation predictions indicate that the inflow to the Karoon4 reservoir would decline in the future periods compared to the base period.

The results for non-adaptive operation show that the reliability of hydropower generation from Pareto solutions in the early, middle, and late periods would be reduced 50, 30 and 63 %, respectively, relatively to those of the base period. The vulnerability of hydropower generation

**Table 5** Optimal adaptive solutions for real-time dynamic operation rules in the middle period (2055–2069)

	$S_I^{middle}$			$S_{II}^{middle}$			$S_{III}^{middle}$		
	$x_1$	$x_2$	$x_3$	$x_1$	$x_2$	$x_3$	$x_1$	$x_2$	$x_3$
Reliability (%)	57.42			48.33			33.89		
Vulnerability (%)	21.71			16.16			14.18		
Jan	-0.0681	0.0571	389.2269	-0.0999	0.1054	397.5340	0.2302	0.2217	210.8179
Feb	-0.0009	0.1741	314.2500	0.0852	0.1777	258.1885	0.0658	0.3427	167.1439
Mar	0.0095	0.2488	192.6147	0.0242	0.2489	197.4758	0.3942	-0.0775	224.0703
Apr	0.1729	0.1103	127.9600	0.1768	0.1095	132.0720	0.0801	0.0991	220.5018
May	0.0926	0.0814	219.5046	0.0979	0.1048	201.9144	0.2295	0.0524	137.8725
Jun	0.3492	-0.0002	54.5916	0.3414	0.0012	63.2849	0.2124	0.1214	96.9162
Jul	0.1747	0.2620	54.0330	0.1748	0.2628	54.0983	0.0718	0.1275	207.0172
Aug	0.0168	0.4688	50.3190	0.0486	0.4583	53.8534	0.2134	0.1793	81.2587
Sep	0.2458	0.2752	85.7174	0.2408	0.2149	90.0688	0.1850	0.2827	55.9790
Oct	0.3286	0.1635	144.3358	0.3487	0.1596	88.5286	0.2336	0.2768	58.6728
Nov	-0.0114	-0.0869	51.1022	0.1374	-0.0552	51.1649	0.4074	0.1962	50.8885
Dec	0.0747	-0.2571	50.1591	0.2518	0.5550	73.3639	0.4697	-0.0074	169.8663

**Table 6** Optimal adaptive solutions for real-time dynamic operation rules in the late period (2085–2099)

	$S_I^{late}$			$S_{II}^{late}$			$S_{III}^{late}$		
	$x_1$	$x_2$	$x_3$	$x_1$	$x_2$	$x_3$	$x_1$	$x_2$	$x_3$
Reliability (%)	27.21			18.33			8.89		
Vulnerability (%)	53.81			46.87			44.71		
Jan	-0.0102	0.0990	53.9236	0.4894	0.0728	93.4803	0.5071	0.0127	50.7414
Feb	-0.1734	0.0043	156.9793	0.8964	-0.7570	196.6361	0.1728	0.3774	50.4865
Mar	0.4423	-0.0541	50.1461	0.8270	-0.6390	113.5196	0.2874	0.1763	73.5183
Apr	0.0657	0.0078	329.2780	0.3393	-0.3062	318.7641	0.3113	0.0303	70.2691
May	0.1656	0.1686	212.7870	0.5709	-0.6104	211.7707	0.0365	0.5121	54.8727
Jun	0.9060	-0.9615	125.1592	0.1194	0.3683	69.2396	0.1054	0.4150	50.6916
Jul	0.5390	-0.3363	75.3237	0.6369	-0.8571	109.5064	0.0005	0.5917	50.4918
Aug	0.2743	-0.8262	65.9907	0.4936	-0.9653	64.8780	0.1362	0.0949	56.4197
Sep	0.1870	-0.9382	50.2202	0.2499	-0.5956	60.5284	0.0247	0.3859	68.0321
Oct	0.4640	0.0778	50.0097	0.1884	-0.8695	53.5649	0.0510	0.0134	50.7020
Nov	0.0002	-0.4031	50.0335	0.2027	-0.9474	52.3050	0.3203	0.1950	53.1799
Dec	-0.0654	-0.0340	50.7278	0.4872	-0.8011	70.4931	0.0987	0.0043	50.2751

from Pareto solutions in the early, middle, and later periods would be increased 28, 18 and 48 %, respectively, relative to the base period. The results from the adaptive operation approach show that the reliability of selected Pareto solution improves 11, 4 and 11 %, respectively and their vulnerability improves 7, 5 and 4 %, respectively relative to non-

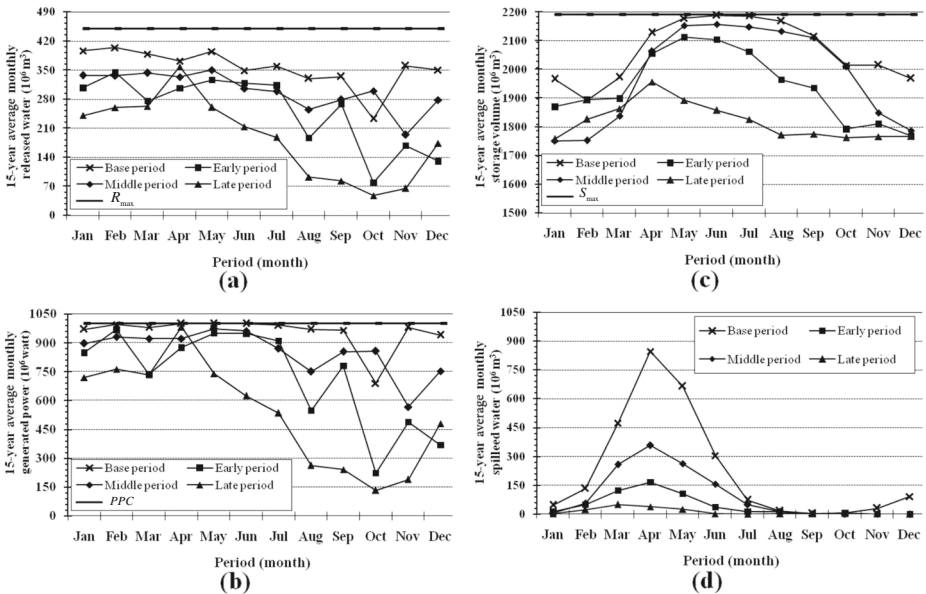


**Fig. 9** Average long-term volume variations of: **a** released water; **b** generated power; **c** storage volume; and **d** spilled water from Pareto solutions for the base, early, middle and late

adaptive operation approach. As a result, it was shown that applying dynamic multi-objective real-time reservoir operation rules would be an effective adaptation approach to climate change.

## References

- Ahmadi M, Bozorg Haddad O, Marino MA (2014) Extraction of flexible multi-objective real-time reservoir operation rules. *Water Resour Manag* 28(1):131–147
- Ashofteh PS, Bozorg Haddad O, Marino MA (2013a) Climate change impact on reservoir performance indexes in agricultural water supply. *J Irrig Drain Eng* 139(2):85–97
- Ashofteh PS, Bozorg Haddad O, Marino MA (2013b) Scenario assessment of streamflow simulation and its transition probability in future periods under climate change. *Water Resour Manag* 27(1):255–274
- Boyer C, Chaumont D, Chartier I, Roy AG (2010) Impact of climate change on the hydrology of St. Lawrence tributaries. *J Hydrol* 384(1–2):65–83
- Bozorg Haddad O, Mariño MA (2011) Optimum operation of wells in coastal aquifers. *Proc Inst Civ Eng : Water Manag* 164(3):135–146
- Bozorg Haddad O, Adams BJ, Mariño MA (2008) Optimum rehabilitation strategy of water distribution systems using the HBMO algorithm. *J Water Supply: Res Technol - AQUA* 57(5):327–350
- Bozorg Haddad O, Moradi-Jalal M, Mirmomeni M, Kholghi MKH, Mariño MA (2009) Optimal cultivation rules in multi-crop irrigation areas. *Irrig Drain* 58(1):38–49
- Bozorg Haddad O, Mirmomeni M, Zarezadeh Mehrizi M, Mariño MA (2010a) Finding the shortest path with honey-bee mating optimization algorithm in project management problems with constrained/unconstrained resources. *Comput Optim Appl* 47(1):97–128
- Bozorg Haddad O, Mirmomeni M, Mariño MA (2010b) Optimal design of stepped spillways using the HBMO algorithm. *Civ Eng Environ Syst* 27(1):81–94
- Bozorg Haddad O, Afshar A, Mariño MA (2011a) Multireservoir optimisation in discrete and continuous domains. *Proc Inst Civ Eng : Water Manag* 164(2):57–72
- Bozorg Haddad O, Moradi-Jalal M, Mariño MA (2011b) Design-operation optimisation of run-of-river power plants. *Proc Inst Civ Eng : Water Manag* 164(9):463–475
- Deb K, Partap A, Agarwal S, Meyarivan T (2002) A fast and elitist multiobjective genetic algorithm: NSGAII. *IEEE Trans Evol Comput* 6(2):182–197
- Diaz-Nieto J, Wibly RL (2005) A comparison of statistical downscaling and climate change factor methods: impacts on low flows in the River Thames, United Kingdom. *Clim Chang* 63(2–3):245–268
- Eum HL, Simonovic SP (2010) Integrated reservoir management system for adaptation to climate change: The Nakdong river basin in Korea. *Water Resour Manag* 24(13):3397–3417
- Fallah-Mehdipour E, Bozorg Haddad O, Mariño MA (2011a) MOPSO algorithm and its application in multipurpose multireservoir operations. *J Hydroinf* 13(4):794–811
- Fallah-Mehdipour E, Bozorg Haddad O, Beygi S, Mariño MA (2011b) Effect of utility function curvature of Young's bargaining method on the design of WDNs. *Water Resour Manag* 25(9):2197–2218
- Fallah-Mehdipour E, Bozorg Haddad O, Mariño MA (2012a) Real-time operation of reservoir system by genetic programming. *Water Resour Manag* 26(14):4091–4103
- Fallah-Mehdipour E, Bozorg Haddad O, Rezapour Tabari MM, Mariño MA (2012b) Extraction of decision alternatives in construction management projects: application and adaptation of NSGA-II and MOPSO. *Expert Sys Appl* 39(3):2794–2803
- Fallah-Mehdipour E, Bozorg Haddad O, Mariño MA (2013a) Developing reservoir operational decision rule by genetic programming. *J Hydroinf* 15(1):103–119
- Fallah-Mehdipour E, Bozorg Haddad O, Mariño MA (2013b) Extraction of multicrop planning rules in a reservoir system: application of evolutionary algorithms. *J Irrig Drain Eng* 139(6):490–498
- Hay LE, Wibly RL, Leavesley GH (2000) A comparison of delta change and downscaled GCM scenarios for three mountainous basins in the United States. *J Am Water Resour Assoc* 36(2):387–397
- Intergovernmental Panel on Climate Change (2000) Emission Scenarios. Cambridge University Press, Cambridge, UK
- Intergovernmental Panel on Climate Change (2014) Climate change 2014: impacts, adaptation, and vulnerability. the 5th assessment report. Cambridge University Press, Cambridge, UK
- Jakeman AJ, Hornberger GM (1993) How much complexity is warranted in a rainfall-runoff model? *Water Resour Res* 29(8):2637–2649
- Jiang T, Chen YD, Xu C, Chen X, Chen X, Singh VP (2007) Comparison of hydrological impacts of climate change simulated by six hydrological models in the Dongjiang Basin, South China. *J Hydrol* 336(3):316–333

- Karimi-Hosseini A, Bozorg Haddad O, Mariño MA (2011) Site selection of raingauges using entropy methodologies. *Proc Inst Civ Eng : Water Manag* 164(7):321–333
- Lee SY, Fitzgerald CJ, Hamlet AF, Burges SJ (2011) Daily time-step refinement of optimized flood control rule curves for a global warming scenario. *J Water Resour Plan Manag* 137(4):309–317
- Loáiciga HA (2002) Reservoir design and operation with variable lake hydrology. *J Water Resour Plan Manag* 128(6):399–405
- Loáiciga HA (2004) Analytic game-theoretic approach to groundwater management. *J Hydrol* 297:22–33
- Loáiciga HA, Valdes JB, Vogel R, Garvey J, Schwarz H (1996) Global warming and the hydrologic cycle. *J Hydrol* 174(1–2):83–128
- Loáiciga HA, Maidment D, Valdes JB (2000) Climate change impacts in a regional karst aquifer, Texas, USA. *J Hydrol* 227:173–194
- Majone B, Bovolo CI, Bellin A, Blenkinsop S, Fowler HJ (2012) Modeling the impacts of future climate change on water resources for the Gállego river basin (Spain). *Water Resour Res* 48(1), W01512
- Minville M, Brissette F, Leconte R (2008) Uncertainty of the impact of climate change on the hydrology of a nordic watershed. *J Hydrol* 358(1–2):70–83
- Minville M, Brissette F, Krau S, Leconte R (2009) Adaptation to climate change in the management of a canadian water-resources system exploited for hydropower. *Water Resour Manag* 23(14):2965–2986
- Mitchell TD (2003) Pattern scaling: an examination of the accuracy of the technique for describing future climates. *Clim Chang* 60(3):217–242
- Muzik I (2001) Sensitivity of hydrologic systems to climate change. *Can Water Resour J* 26(2):233–253
- Noory H, Liaghat AM, Parsinejad M, Bozorg Haddad O (2012) Optimizing irrigation water allocation and multicrop planning using discrete PSO algorithm. *J Irrig Drain Eng* 138(5):437–444
- Orouji H, Bozorg Haddad O, Fallah-Mehdipour E, Mariño MA (2013) Estimation of Muskingum parameter by meta-heuristic algorithms. *Proc Inst Civ Eng : Water Manag* 166(6):315–324
- Pope VD, Gallani ML, Rowntree PR, Stratton RA (2000) The impact of new physical parameterizations in the Hadley Centre climate model: HadAM3. *Climate Dynamic* 16(2–3):123–146
- Seifollahi-Aghmiuni S, Bozorg Haddad O, Omid MH, Mariño MA (2011) Long-term efficiency of water networks with demand uncertainty. *Proc Inst Civ Eng : Water Manag* 164(3):147–159
- Seifollahi-Aghmiuni S, Bozorg Haddad O, Omid MH, Mariño MA (2013) Effects of pipe roughness uncertainty on water distribution network performance during its operational period. *Water Resour Manag* 27(5):1581–1599
- Shokri A, Bozorg Haddad O, Mariño MA (2013) Algorithm for increasing the speed of evolutionary optimization and its accuracy in multi-objective problems. *Water Resour Manag* 27(7):2231–2249
- Shokri A, Bozorg Haddad O, Mariño MA (2014) Multi-objective quantity–quality reservoir operation in sudden pollution. *Water Resour Manag* 28(2):567–586
- Wilby RL, Harris I (2006) A framework for assessing uncertainties in climate change impacts: low-flow scenarios for the River Thames, UK. *Water Resour Res* 42(2), WR004065
- Young HP (1993) An evolutionary model of bargaining. *J Econ Theory* 59(1):145–168
- Yu PS, Yang TC, Wu CK (2002) Impact of climate change on water resources in southern Taiwan. *J Hydrol* 260(1–4):161–175
- Zhou Y, Guo S (2013) Incorporating ecological requirement into multipurpose reservoir operating rule curves for adaptation to climate change. *J Hydrol* 498:153–164